Applied Energy 131 (2014) 97–107

Contents lists available at ScienceDirect

Applied Energy

journal homepage: www.elsevier.com/locate/apenergy

Electro-thermal analysis and integration issues of lithium ion battery for electric vehicles

L.H. Saw, Y. Ye, A.A.O. Tay *

Department of Mechanical Engineering, Faculty of Engineering, National University of Singapore, 117576 Singapore, Singapore

HIGHLIGHTS

- We modeled the electrical and thermal behavior of the Li-ion battery.
- We validated the simulation results with experimental studies.
- We compared the thermal performance of different size of cylindrical cells.
- We investigated the integration issues of cylindrical cells into battery pack.

ARTICLE INFO

Article history:
Received 14 March 2014
Received in revised form 9 May 2014
Accepted 13 June 2014
Available online 7 July 2014

Keywords:
Battery temperature
Electric vehicles
Lithium iron phosphate
Cell integration
Battery model

ABSTRACT

Electrical and thermal characteristics of lithium-ion battery packs in electric vehicles in different operating conditions are important in order to design the battery pack thermal management system. In this work, electrical and thermal behaviors of different size of $LiFePO_4$ cylindrical cells are investigated under various operating conditions. The simulation results show good agreement with the experimental data under various operating modes. Due to the large thermal resistance of layered active material in a Li-ion cell, the temperature difference in the radial direction is significantly correlated with a diameter of cell and I_t-rates. Compared with natural convection, strong forced convection will reduce the temperature uniformity in the cell and accelerate the thermal aging rate. Lastly, integration issues of the cells into a battery pack are discussed from mechanical, electrical, thermal, control and monitoring, manufacturing and maintenance aspects. These issues could impact the performance, cost, driving range and life cycle of the battery pack in electric vehicles.

1. Introduction

Li-ion batteries are rechargeable batteries which are gaining popularity for Electric Vehicles (EVs) and Hybrid Electric Vehicles (HEVs) applications. Li-ion batteries with high energy density, low maintenance, less toxic, good cycle life and capable of accepting high charging rate is suitable for energy storage system in EVs and HEVs. Moreover, Li-ion batteries have no memory effect, do not required periodic deliberate full discharge and the self-discharge rate is less than half of Nickel Cadmium (NiCd) and Nickel Metal Hydride (NiMH) batteries. Hence, Li-ion batteries have been extensively investigated for potential applications in EVs and HEVs to replace NiMH and lead acid battery which have low energy density and depth of discharge. Recently, a series of fire accidents involving Li-ion battery pack in EVs indicated that there are still many challenges to be overcome, especially thermal issues of Li-ion battery. Li-ion battery needs to operate between 25 °C–40 °C to maximize its performance, cycle life and reduce capacity fading caused by thermal aging [1]. Cycle life and capacity of the Li-ion battery are inverse proportional to the temperature of the cell [2,3]. In order to satisfy the power requirements for specific devices, Li-ion batteries are electrically connected in series and or parallel to form a pack. Therefore, the uniformity of the cell temperature in the large pack should be maintained as homogeneous as possible (3–5 °C) to ensure comparable power performance, effective cell balancing and charge acceptance during regenerative braking [4]. Therefore, an accurate battery model is needed in order to predict the temperature of the battery pack when the physical battery testing facility is not available. Battery model has several advantages such as estimation of electrical and thermal behavior under different driving conditions in a short time, reduce the product life cycle cost of the battery pack and testing equipment cost [5]. The battery model is particularly useful for battery pack thermal management system and battery pack control and monitoring design and planning.

* Corresponding author. Tel.: +65 65162207; fax: +65 67791459.
E-mail address: mpetayao@nus.edu.sg (A.A.O. Tay).

http://dx.doi.org/10.1016/j.apenergy.2014.06.016
0306-2619/

Nomenclature

A	exponential voltage, V
A_s	external surface area of the cell, m^2
A_{mf}	cross section flow area for cooling air per module, m^2
A_{ms}	total module surface area exposed to cooling air, m^2
B	exponential zone time constant, $(Ah)^{-1}$
CFM	Cubic feet per minute
C_p	specific heat capacity of the battery, J kg^{-1} K^{-1}
C_{bp}	theoretical capacity of the battery, Ah
E	emissivity
E_0	battery constant voltage, V
h	convective heat transfer coefficient, W m^{-2} K^{-1}
I_t	discharge current in amperes during 1 h discharge
i	battery current, A
i^*	filtered current, A
K	polarization constant, $V(Ah)^{-1}$ or polarization resistance, Ω
λ	conductive heat transfer coefficient
$\dot{m}$	mass flow rate of air, kgs^{-1}
Q	battery capacity, Ah
R_{int}	internal resistance, Ω
R_c	terminal contact resistance, Ω
T	temperature of battery, K
T_∞	free stream temperature of air, K
t	time, s
V_{batt}	battery voltage, V
ρ	density of the battery, kg m^{-3}
ρ_{air}	density of the air, kg m^{-3}
σ_{sb}	Stefan–Boltzmann constant, W m^{-2} K^{-4}

Subscripts

exp	exponential
nom	nominal
full	fully charged
max	maximum
forced	forced convection

Superscript

k	Peukert constant

Several Li-ion battery models have been proposed to predict the charging and discharging behavior, state of charge (SOC), chemical reaction, Li-ion distribution, current density distribution, heat generation, temperature distribution, etc. Li-ion battery models can be distinguished into two major groups, mechanistic models – electrochemical, thermal models and empirical models- equivalent circuit models. Electrochemical modeling [6–10] used a coupled time variant spatial partial differential equations to model the electrochemical reaction of the battery. Although electrochemical models can accurately predict the aging and thermal behavior of Li-ion battery, the equations itself are complex and require extensive computational resources [11]. Moreover, most of the studies only presented results of numerical simulations and did not validate with experimental work [12–15].

The electrical model [16–27] or equivalent electric circuit consists of the voltage source, resistors and capacitors or set of empirical equations to represent the electrical behavior of a battery. The open circuit voltage of the battery is defined as a function of the SOC. The parameters required for the model are extracted from the Hybrid Pulse Power Characterization test (HPPC), pulse discharging or low I_t-rate of constant current discharging curves. These models are easy to use and required shorter computational times and have an advantage in large system simulations, especially in analyzing dynamic and thermal behavior of the battery under different driving cycles.

Lithium iron phosphate (LFP) battery have high thermal runaway temperature (270 °C), non-toxic, do not release oxygen at elevated temperatures and high cycle life (1000–2000) as compared to $LiCoO_2$, $LiMnO_4$ and $LiNiMnCoO_2$ has make it become an attractive solution for future EVs battery pack [28]. Although there are some studies have been carried out to investigate the thermal behavior of Li-ion battery under different driving cycles, modeling work on LFP cell are rare [20,29–31].

Li-ion batteries can be constructed into various shapes and sizes for different applications: spiral wound to form cylindrical cells or stacked plates to form pouch cells. The fabrication technology of spiral wound design of the Li-ion battery is more mature and commonly found in the market. Besides, spiral wound design has several advantages as compared to prismatic and pouch cell design such as: easy to fabricate, high energy density, mechanical stability, incorporated safety vent and not prone to swelling during operation [32]. However, small specific area to volume of a cylindrical battery could lead to the development of a large temperature gradient in the cell and thermal aging issues, heat is retained in the cell and hot spots are formed in the center of the cell. Large temperature gradient developed across the cell at large load could cause capacity fading [33]. The temperature gradient in the cell is significantly correlated with the diameter of the cell and I_t-rates. This implies that thermal analysis of different sizes of cylindrical cell is necessary to provide a guideline for determining a suitable size to integrate into EVs or HEVs battery pack.

In the present work, an electrical–thermal battery model was developed to investigate the electrical performance and thermal behavior of two different sizes of spiral wound LFP cell. The simulation results are confirmed by experimental data. The development of internal temperature under different cooling conditions was predicted by the battery model. Next, the validated single cell model is then extended to the whole battery pack to examine the thermal response of the cell under US06 Supplemental Federal Test Procedure (SFTP) driving cycle. Furthermore, the integration issues of the cell into the battery pack are discussed from different points of view, such as mechanical, electrical, thermal, manufacturing and maintenance. This study will serve as a basic guideline for cell thermal management system design and integration of cell for EVs and HEVs battery pack.

2. Model development

2.1. Battery model

A battery model is needed to describe the correlation between the input parameters to the Li-ion battery such as current or power and outputs of the battery model like voltage, SOC for constant current charging/discharging and dynamic conditions. The modified Shepherd model was used to model the voltage dynamics of the LFP cell in this study [34–36]. Eqs. (1) and (2) are used to model the charging and discharging characteristics of the battery respectively [35,36]. In this model, the internal resistance of the cell was assumed to be constant and does not change with SOC and temperature. Moreover, the battery model was treated as independent of the temperature and the model parameters for charging and discharging are identical and the hysteresis phenomenon was not

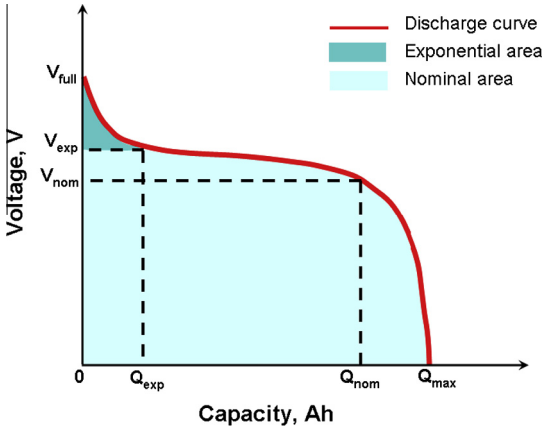

Fig. 1. Typical discharge characteristic of Li-ion battery [35,36].

modeled in this study. The battery model parameters E_0, K, A and B were extracted from the battery discharge curve of 0.2 I_t as in Fig. 1 in according to the procedures proposed by Tremblay et al. [35,36]. Filter current is used to model the slow dynamic behavior of cell voltage and solve the algebraic loop problem in Simulink [35].

Charging ($i^* < 0$)

$$V_{batt} = E_0 - R_{int}\cdot i - K\frac{Q}{it - 0.1\cdot Q}\cdot i^* - K\left(\frac{Q}{Q-it}\right)it + Aexp(-B\cdot it) \quad (1)$$

Discharging ($i^* > 0$)

$$V_{batt} = E_0 - R_{int}\cdot i - K\frac{Q}{Q-it}\cdot i^* - K\left(\frac{Q}{Q-it}\right)it + Aexp(-B\cdot it) \quad (2)$$

The voltage of the cell at fully charged state is defined in Eq. (3) [35,36].

$$V_{full} = E_0 - R_{int}\cdot i + A \quad (3)$$

The voltage at the exponential section is defined in Eq. (4) [35,36].

$$V_{exp} = E_0 - K\frac{Q}{Q-Q_{exp}}\cdot(Q_{exp}+i) - R_{int}\cdot i + Aexp\left(\frac{-3}{Q_{exp}}\cdot Q_{exp}\right) \quad (4)$$

The voltage of the cell at the nominal zone is defined in Eq. (5) [35,36].

$$V_{nom} = E_0 - K\frac{Q}{Q-Q_{nom}}\cdot(Q_{nom}+i) - R_{int}\cdot i + Aexp\left(\frac{-3}{Q_{exp}}\cdot Q_{nom}\right) \quad (5)$$

2.2. Thermal model

In this study, the physical properties of the battery are assumed uniform and not affected by temperature. General energy balance as in Eq. (6) proposed by Bernardi et al. was used to identify the total heat generated in the cell [37]. The source of heat generated in the cell comprises joule heat and reversible heat. The reversible heat term is calculated using the relation of dU/dT with the SOC proposed by Forgez et al. [38]. In addition, contact resistance has been added in the equation to improve the prediction of the heat generation.

$$Q_{gen} = i\left(E_0 - V_{batt} + T\frac{dU}{dT}\right) + i^2R_c \quad (6)$$

The general energy balance equation for the battery thermal model is given by:

$$\rho C_p\frac{dT}{dt} = \lambda\frac{\partial^2 T}{\partial r^2} + Q_{gen} \quad (7)$$

With boundary conditions at the outer surface of the cell ($r = R$) is defined by

$$-\lambda\left.\frac{\partial T}{\partial r}\right|_{r=R} = h(T - T_\infty) + E\sigma_{sb}(T^4 - T_\infty^4) \quad (8)$$

2.3. Battery pack thermal model

Modeling of EV is based on Hyundai Trajet and the battery pack is designed using 38,120 cells to provide similar power capacity as in previous studies [28]. Axial air cooling architecture was used to investigate the thermal response of the EV battery pack [28]. The battery pack comprised 28 modules and each module is constructed using 28 pieces of 38,120 cells. Modules in the battery pack are subjected to equal amount of cooling air as shown in Fig. 2. Hence, it is sufficient to study the thermal response of a single module. SFTP driving cycle is more aggressive than Urban Dynamometer Driving Schedule (UDDS) and The Highway Fuel Economy Test (HWFET) and more energy is being charged to and discharged from the battery pack and more heat is generated. Therefore, it was chosen for analyzing the thermal response of the battery pack and benchmark with 18,650 cell battery pack. Thermostat feature was included in the battery model with switching on the temperature set at 35 °C. After the cell temperature reaches 35 °C, the blower will come into deliver 10, 25 or 100 CFM of cooling air per module. The specific parameters of the EV used for driving cycle simulations are tabulated in Table 1.

2.4. Experimental setup and battery model parameters extraction

Two different sizes of commercial cylindrical LFP cell were examined in the present study. The details of the cells are given in Table 2. Battery cycler (Maccor Instrument 4000) was used to charge and discharge the battery to obtain the voltage and current curve in function of time. 2.3 V was used as the cutoff voltage for constant current discharging while charging of the batteries were done in two modes: constant current charging until 3.65 V at 0.1 I_t followed by constant voltage charging until the current dropped to 0.01 A. Slow charging is desired to ensure the chemical process within the cell occurs at a rate similar rate for the transfer of electric energy in the isothermal state. The batteries were put at rest for 1 h to ensure the temperature of the battery is in equilibrium with room temperature and the open circuit voltage of the cell is stable. Impedance analyzer (Solartron analytical 1400) was used to assess the internal resistance (R_{int}) of the batteries. The parameters for 38,120 and 18,650 battery models are provided in Table 2.

The surface temperature of the batteries was measured with twelve thermocouples (T-type) attached to different locations of the cell. Three thermocouples were attached in the axial direction and four sides of the battery surface. The experiments were conducted at room temperature of 25 °C under natural convection. Temperature readings were recorded using the HP34970A data acquisition system. The specific heat capacity of the cell was measured using adiabatic accelerating rate calorimeter (THT ARC) as shown in Table 2.

2.5. Numerical procedures

The electro-thermal model of the battery was developed using Matlab-Simulink 2011b. Electrical and thermal response of the

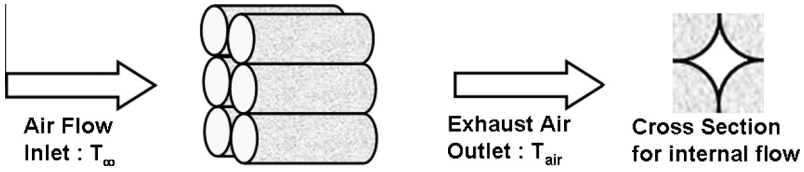

Fig. 2. Schematic of active air cooling system of an EV battery pack [17].

Table 1
Vehicle and cooling system specific parameters for 38,120 cell.

Parameter	Value
Vehicle mass, kg	1828
Frontal area, m^2	3.238
Coefficient of drag, Cd	0.35
Electric motor	75 kW, 200 Nm max
Battery pack	19.5 kWh
Number of cell per module	28
Number of module	28
A_{mf} per module, m^2	0.00868
A_{ms} per module, m^2	0.401
Mass flow rate of cooling air for battery pack, cfm	280, 700, 2800
Surrounding temperature, °C	30

Table 2
Details of LFP cells used in this study.

Parameters	Cell	
	18,650	38,120
Nominal voltage, V	3.2	3.2
Nominal capacity, mAh	1300	8000
Cathode material	$LiFePO_4$	$LiFePO_4$
Anode material	Graphite	Graphite
Terminal connector	Spring loaded	Screw
Diameter, m	0.018	0.038
Length, m	0.065	0.0146
Weight, kg	0.030	0.355
Specific heat, J kg^{-1} K^{-1}	900	998
E_0, V	3.21	3.27
R, Ω	0.03	0.0034
K, Ω or V$(Ah)^{-1}$	0.0119	0.00216
A, V	0.2711	0.0854
B, $(Ah)^{-1}$	152.130	23.097

battery model was extracted and compared with the experimental results of constant current discharging and Simplified Federal Urban Driving Schedule (SFUDS) dynamic power profile. Next the validated battery model is further extended to investigate the thermal response of the battery pack for a converted EV under US06-SFTP driving cycle.

2.6. Cell selection for EV battery pack

The electro-thermal model results of 38,120 cell and 18,650 cell will be used to determine the suitable cell for EV battery pack. The benchmarking process is based on Hyundai Trajet and thermal response of the battery pack is assessed the electro-thermal model under US06-SFTP driving cycle. The details of the results are provided in Section 3.6.

3. Results and discussion

3.1. Validation of the cell voltage

Calibration result of the 38,120 battery model using 0.2 I_t of discharge curve is shown in Fig. 3(a) while the error of prediction is given in Fig. 3(b). The highest error of the simulation results as

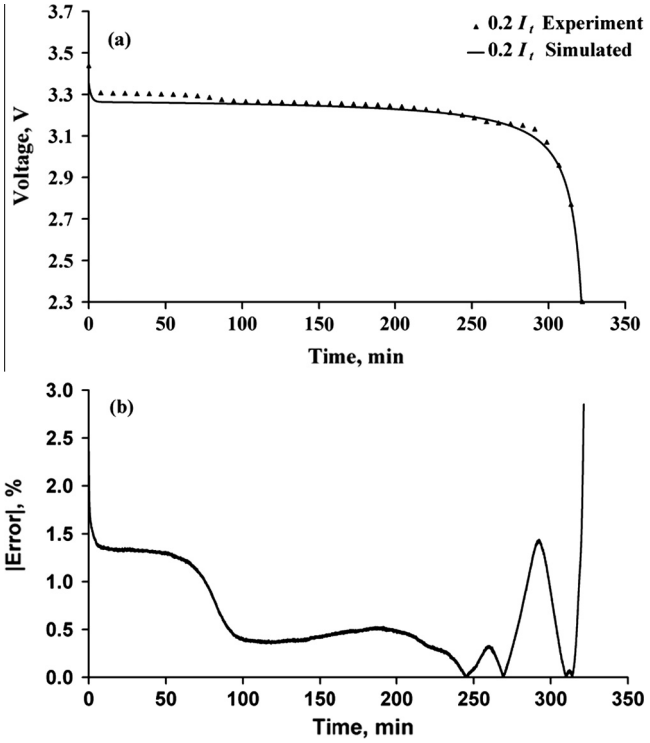

Fig. 3. (a) 38,120 cell voltage during discharge at 0.2 I_t to extract the model parameters. (b) Error of voltage prediction.

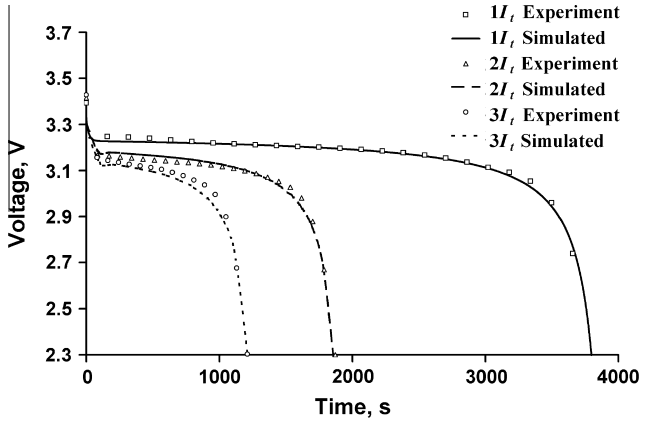

Fig. 4. Comparison of simulated and experimental data at 1, 2 and 3 I_t-rates.

compared to experimental data is about −0.06 V during initial discharge, while at the end of discharge it is less than 3%. In Fig. 4 the measured and simulated voltage for 38,120 cell during 1, 2 and 3 I_t-rate of discharge is shown. Comparisons of simulated and measured voltage show that the battery model provides a good estimation of the electrical behavior of the cell at various I_t-rates. Average squared error for 1, 2, 3 I_t-rates are 0.0000260, 0.0000419 and 0.000117 respectively. Discharging at high I_t-rates

could cause a rise in cell temperature. In addition, internal resistance of the cell is dependent on temperature, thus the error of prediction at 3 I_t is slightly larger as compared to 1 and 2 I_t-rates. Although the cell nominal rating is 8 Ah, the final capacity resulted from 1 I_t of discharge could reach 8.6 Ah. The final capacity at the end of 3 I_t of discharge is about 8.4 Ah which is about 3.5% less than the capacity at 0.2 I_t (8.7 Ah). On the other hand, at 3 I_t discharge of 18,650 cell suffered more capacity loss which is about 8% as compared to its capacity of 0.2 I_t [32].

3.2. Evolutions of the cell temperature and heat generation

Simulated and measured average skin temperature of 38,120 cell at different I_t-rates of discharging under natural convection (5 W m^{-2} K^{-1}) is shown in Fig. 5. The results showed that at high I_t-rates of discharging, temperature rise of the cell are significant. The skin temperature of the cell could rise to 13.8 °C at 3 I_t-rate and the cell exhausted its energy in 20 min. Natural convection is no longer sufficient to keep the cell temperature within safe operating limits. Therefore, a battery thermal management system is required in this situation. The averaged squared error of the experiments data and simulation results for 1, 2 and 3 I_t-rates of discharging are 0.0888, 0.0224 and 0.0143 respectively. At 3 I_t of discharge, the skin temperature of the 38,120 cell is about 6 °C less than 18,650 cell at a similar rate of discharge. Heat exchange surface area per unit jelly roll volume of the cell is a critical factor to determine the heat dissipation rate from the cell to the environment [39]. The heat transfer area per unit volume of 18,650 and 38,120 cells is 222.22 m^{-1} and 105 m^{-1} respectively. As the ratio of surface area to volume decrease, the heat transfer ability of the cell was reduced and the internal temperature of the cell is increased [9]. Although the skin temperature of the 38,120 cell is lower than 18,650 cell, more heat is trapped inside the cell. Therefore, the smaller cell will have a higher skin temperature at a similar I_t-rate of charging and discharging. Sometimes, this will give false information to the user that a large cell performs better than a smaller cell in the thermal aspect.

Estimated total heat generation of 38,120 battery is depicted in Fig. 6. 6.5 W, 14 W and 20 W per cell of heat were generated toward the end of 1–3 I_t-rate of discharge respectively. Heat generated from the battery is also positively correlated to the size and capacity of the cell. Heat generated from 18,650 cell is only 9% of 38,120 cell at 1 I_t of discharge, while the heat generated at 3 I_t is about 15% of 38,120 cell in a similar I_t-rate of discharge [28].

3.3. Internal temperature of cell

Temperature distribution of 38,120 and 18,650 cells under different cooling conditions at the end of 3 I_t of discharge is

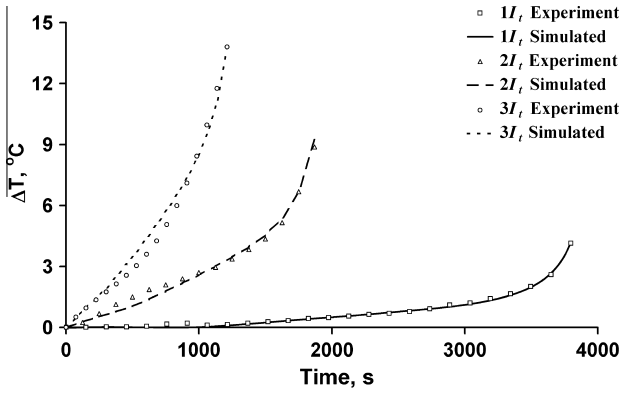

Fig. 5. Temperature rise of the battery during discharge at 1, 2 and 3 I_t-rates.

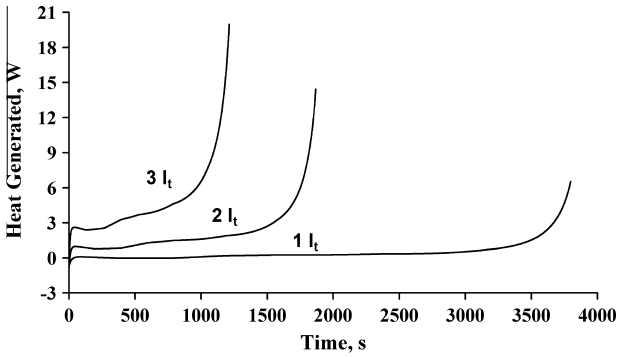

Fig. 6. Heat generated of 38,120 cell during discharge at 1, 2 and 3 I_t-rates.

provided in Fig. 7. Due to the anisotropic nature of layered active material inside the battery, the temperature distribution in the axial direction of the cell is fairly uniform [39] and a temperature gradient is expected only in the radial direction of the cell. Heat shrink film which is used for insulation of the metal casing will prevent the heat generated in the cell from being effectively dissipated to the environment. Therefore, a temperature jump was found between the insulator and metal casing of the cell as shown in the initial and end section as in Fig. 7. The maximum temperature region of the cell is located in the active material region near the hollow core. The hollow core situated at the center of the cell is a product of the cell manufacturing process. During cell sealing process, an electrolyte will be injected into the active material and the hollow core will be filled with the electrolyte as well. An attempt to measure the internal temperature of the cell at the hollow core region may not produce any useful information on the maximum temperature of the cell [38,39]. As shown in Fig. 7, the temperature in the hollow core region is lower than the active material near the hollow core region. 5 °C of temperature gradient was developed in 38,120 cell during 3 I_t of constant current discharge under natural convection as shown in Fig. 7(a). The maximum internal temperature of the cell may reach 44 °C for 3 I_t of constant current discharge. On the other hand, the temperature gradient in the 18,650 cell is also 5 °C under natural convection (5 W m^{-2} K^{-1}) and the maximum temperature in the active material region is about 50 °C. The temperature gradient of the cell will grow when strong forced convection is used to cool. When the heat transfer coefficient increase 500 W m^{-2} K^{-1}, the temperature gradient for 38,120 and 18,650 cell may rise to 14 °C and 16 °C respectively as shown in Fig. 7. Opposite to excellent thermal conductivity of metal casing, the active material region is a poor thermal conductor. Although the current collectors of the cell are made of copper and aluminum, but porous electrodes and separators are poor conductors. The main function of a separator is to isolate the anode and the cathode layer while providing an effective transport medium for Li-ion. Poor thermal properties of the separator will prevent the heat from being effectively dissipated to the outer environment and it further proves that heat flux inside the large cell is not always outward [39]. Therefore, the safety of the battery cannot be simply determined by measuring the skin temperature of the cell. Using strong forced convection to cool the cell is not encouraged as this will introduce undesirable temperature gradient in the cell and accelerate the thermal aging. In the open literature, there are various types of degradation models used to investigate the cycle life of the battery [40–42]. In the current study, thermal aging model proposed by Wang et al. is adopted and the thermal aging of the $LiFePO_4$ cell can be represented by the Arrhenius equation as below [40]:

$$Q_{loss} = 30330 exp\left(\frac{-31500}{8.314 \cdot T}\right) A_h^{0.552} \quad (9)$$

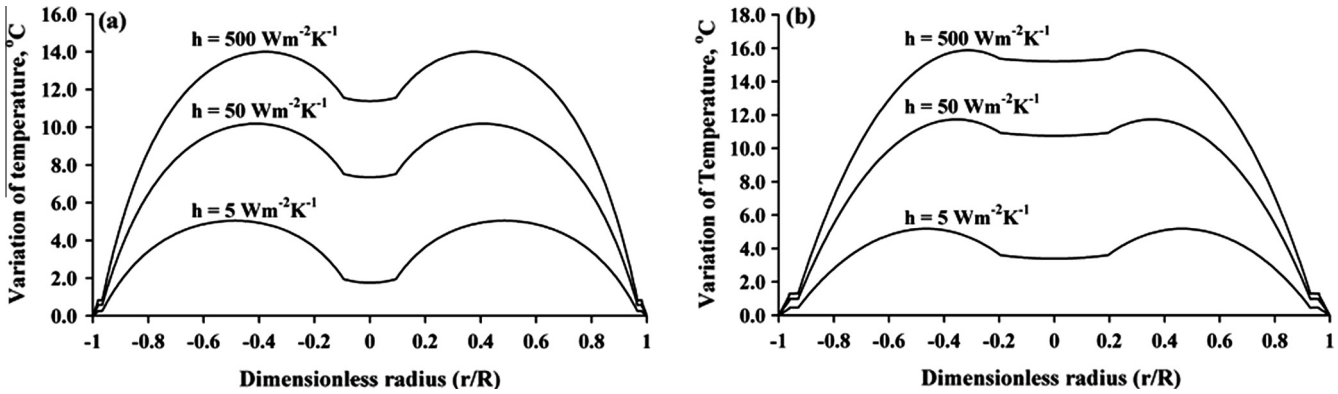

Fig. 7. Predicted variation of internal temperature of the cell. (a) 38,120 cell. (b) 18,650 cell at 3 I_t-rates.

The capacity loss of the cell at 30 °C, 40 °C, 50 °C and 60 °C for total of 1000 Ah throughput is 5.12%, 7.65%, 11.12% and 15.81% respectively. This further indicates that 10 °C of temperature difference will lead to additional 3–5% reduction in the cycle life of the cell. Compared to strong convection cooling of the battery outer surface, improving the thermal properties of the separator and internal structure of the cell or filling the hollow core with heat absorbing medium is more effective in improving the heat dissipation of the cell.

3.4. Dynamic behavior of the cell under SFUDS

Validation of battery model dynamic behavior required comparison with an independent set of series charging and discharging test. SFUDS, featuring 360s of repeating charging and discharging at certain specific power was used for this study [28]. The voltage and current response plot of the simulated results and the experimental measurement of 38,120 cell in the first 360s are depicted in Fig. 8. The error graph shows that the discrepancy between the model and experiment for the voltage is below 0.5% and below 2% for the current. Fig. 9 shows both experimental and simulated voltage and temperature profile of 38,120 cell under 450 min of SFUDS cycle. The voltage drops to the lowest point during 79 W/kg specific power discharge within each sub-cycle of 360s. The voltage of the cell decreases with the number of sub-cycles and oscillates in a pulse with the power pulses. The voltage of the cell gradually decreases as the SOC of the cell ceases to cut off voltage to maintain the power requirement of the cycles. A good agreement can be observed between the simulated and experimental results. Total heat generated for 450 min of a SFUDS test of 38,120 cell is about 106 J which can be effectively dissipated by natural convection and the overall change of the cell skin temperature is within 1 °C. Endothermic heat generation is observed during the initial 280 min of the cycle. Then, the heat generation

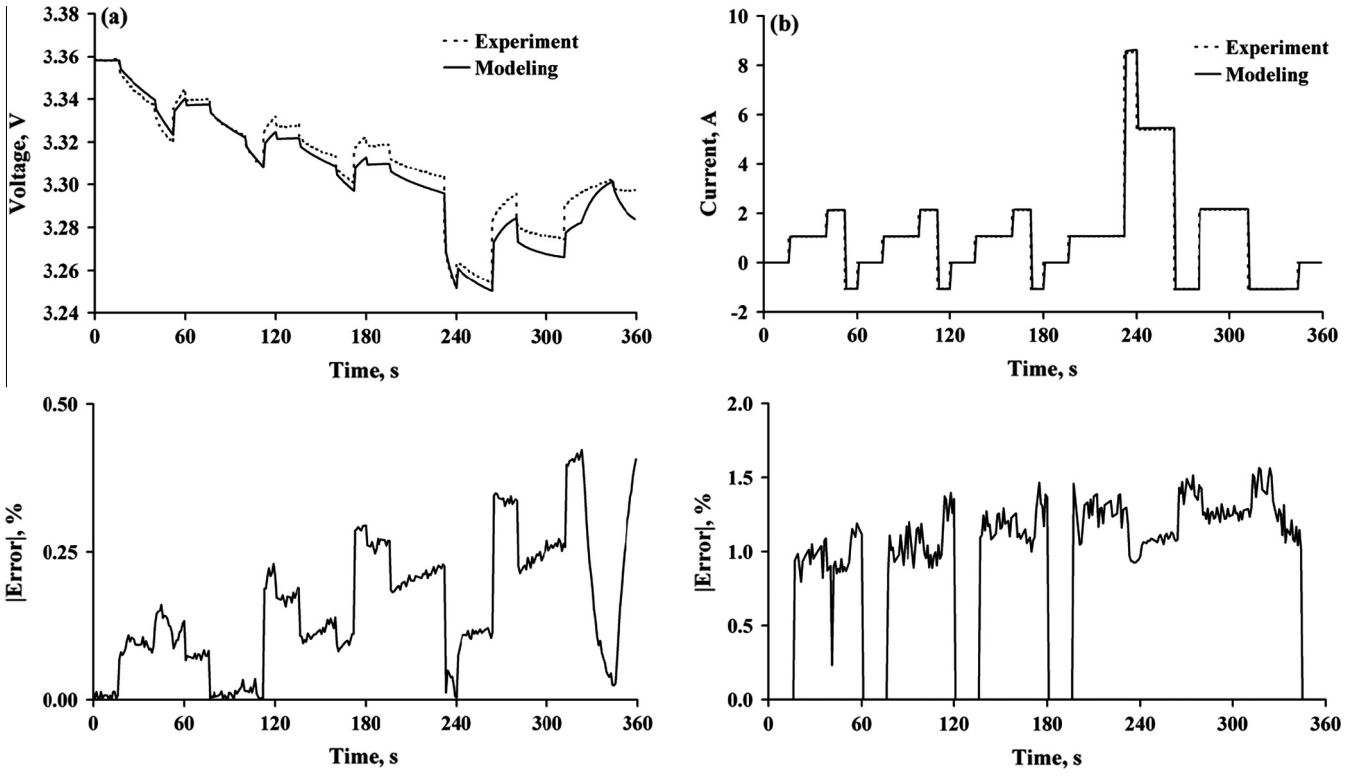

Fig. 8. Validation of battery model using SFUDS (a) Voltage, and (b) current.

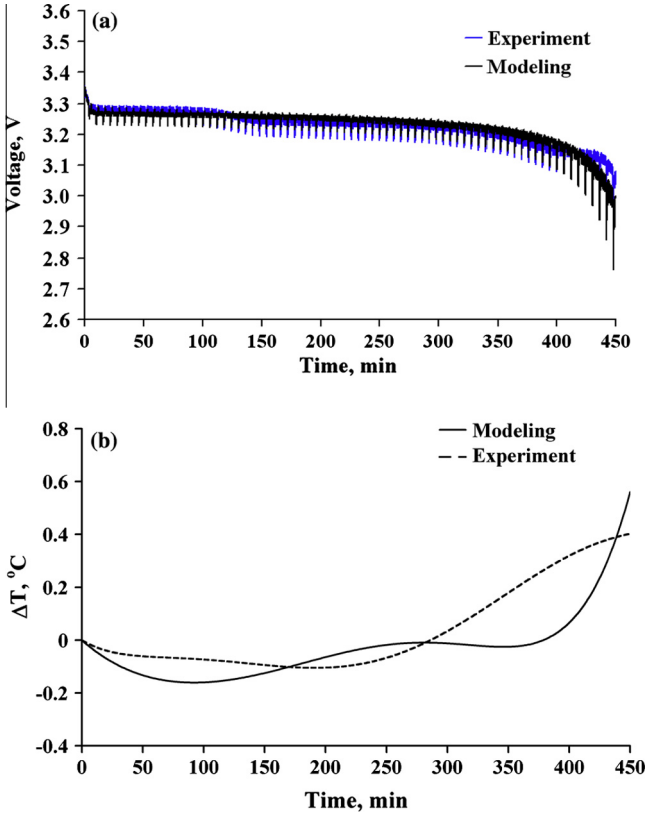

Fig. 9. Comparison of experiment and modeling results for 450 min of SFUDS profile. (a) Voltage, and (b) temperature.

rate gradually increased and became exothermic as the charging and discharging process continued, contributing to the rise of the overall cell temperature. Therefore, the battery model is crucial to provide an insight of battery state during testing in an economic and nondestructive way without over-charging or over-discharging of the cell.

3.5. Thermal response of the battery pack under US06 driving cycle

Thermal response of the 38,120 cell battery pack under US06 driving cycle is shown in Fig. 10. The battery pack is subjected to 600s of the repeated US06 cycle until the voltage of the battery pack reached 64 V. 38,120 cell battery pack is able to complete 4.5 cycles of US06 and deliver power for 45.1 min. Temperature of cells increase continuously in the cycling process and reaches the maximum at the end of the cycle. At the end of the cycle, the average temperature of the battery in the module is 38.1 °C, 37.6 °C and 36 °C for 10 CFM, 25 CFM and 100 CFM of air flow per module respectively. The total flow rate of air is 280, 700 or 2800 CFM for 38,120 cell battery pack which consists of 28 modules. As compared to 18,650 cell battery pack in the previous study [28], 38,120 cell battery pack has higher energy used, higher energy gained from regenerative braking and higher capacity. The heat generated from 38,120 cell module is not as intensive as compared to 18,650 cell module in the previous study [28]. As shown in Table 3, heat generated from 38,120 cell battery pack is about 33% less than the 18,650 cell battery pack. This is caused by additional heat generated from the contact resistance of spring loaded terminal connector for 18,650 cells. On the contrary, screw connector is used for 38,120 cells to connect the cell and the contact resistance is very low (~0.6 miliohm), only 0.45 kJ of heat is generated by the contact resistance throughout the cycle for 38,120 cell battery pack. On the other hand, the effect of contact resistance of 18,650 cell pack contributed 0.764 MJ of heat generated.

At initial 2200s, natural convection is sufficient to dissipate the heat generated from the 38,120 cell battery pack in the US06 cycle. The blower came in after 2200s (3.6 cycles) to supply cooled air to chill the cells and attempt to bring down the cell skin temperature to below 35 °C. Conversely, skin temperature of 18,650 cell reached 35 °C as soon as 1.2 cycles (744s) of the US06 cycle were completed. Cross section flow area for cooling air per 38,120 cell module is 0.00868 m^2 and is about twice the flow area of 18,650 cell module. Hence, mass flow rate of cooling air for 38,120 cell module need to be double to achieve a similar cooling condition as 18,650 cell module. Although the blower is only operated for 8.3 min, large mass flow of air (2800 CFM per pack) is needed to suppress the temperature rise of the cell. In this case, huge blower is needed and this will increase the cost and power consumption of the pack thus reducing the driving range of the EV.

Gradient of internal cell temperature under strong forced convection, 25 CFM for 18,650 cell module and 100 CFM for 38,120 cell module was investigated. As shown in Fig. 11, gradient of the 38,120 cell internal temperature could reach 6 °C, although there

Table 3
Energy distribution for US06 cycle per pack.

Cell	Discharging, MJ	Charging, MJ	Heat generation, MJ
18,650	58.99	5.71	4.937
38,120	75.73	7.40	3.319

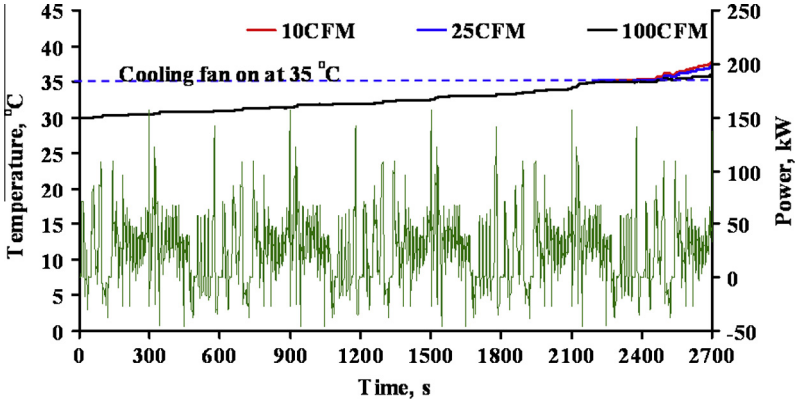

Fig. 10. Thermal response of 38,120 battery pack under US06 driving cycle.

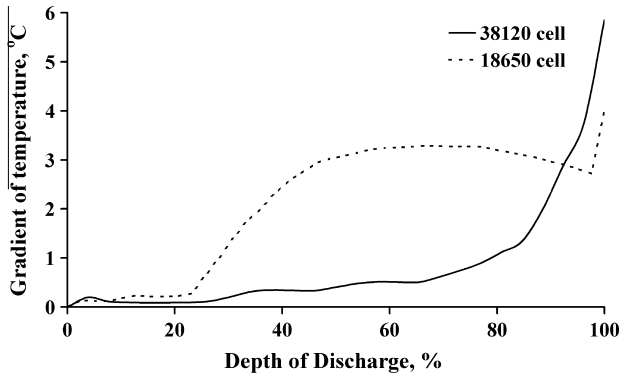

Fig. 11. Gradient of cell internal temperature for US06 driving cycle under maximum cooling capacity.

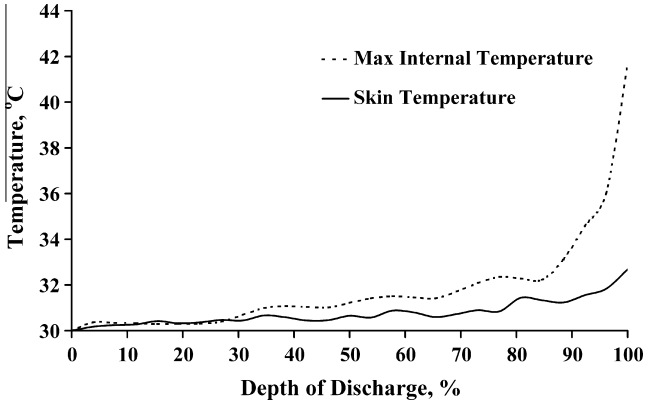

Fig. 12. Cell skin temperature and maximum internal temperature of 38,120 cell under laminar flow of ethylene glycol.

is only 4 °C of temperature difference was developed in the 18,650 cells at the end of the US06 cycle. The internal temperature of 18,650 cell and 38,120 cell could reach 38 °C and 39 °C respectively. Hence, a cell with a larger diameter will have a larger temperature gradient as compared to a small cell.

The effect of using liquid cooling on the 38,120 cell battery pack was also investigated. For closed pack architecture of 38,120 cell module, laminar flow of ethylene glycol is sufficient to maintain the temperature rise of the cell surface below 5 °C as illustrated in Fig. 12. Although the skin temperature of 38,120 cell is successfully maintained at 33 °C, large temperature gradients develop inside the cell. The internal temperature of the cell could reach 42 °C which brings adverse effect to the cell cycle life and accelerates the thermal aging of the cell.

On the other hand, immersion cooling using 3 M Novec 7000 engineering fluid or Fluorinert electronic liquid could be a solution for thermal management of large Li-ion cell. The cells are immersed in the liquid and take advantage of large latent heat of evaporation of the liquid to achieve cooling purpose.

3.6. Cell selection and integration issues of EV battery pack

The selection and integration of cells to form a battery pack are important to determine the safety, durability, life cycle, driving range, cost and fuel economy of the EVs or HEVs. Poor integration of cells may lead to disadvantages such as low performance of the battery pack, shorter cycle life, safety hazard and unnecessary production costs [43,44]. There are several issues associated with the integration of cells into a battery pack, and this involves the mechanical, electrical, thermal, control and monitoring, packaging, manufacturing, maintenance and repair aspects. These issues are important to create a comfortable environment to bring out the best of the cells. Some automakers prefer using a large number of small cells for battery pack while others prefer using a few large cells. For example, Tesla Roadster used more than 7000 18,650 cells (3100 mAh) for their Tesla Model S while Mitsubishi used 88 much larger cells (50 Ah) for their Mitsubishi i-MiEV. Using a larger number of small cells or a small number of large cells has its own advantages and disadvantages. The advantages of using small cells include cost efficiency, a lack of thermal aging tendency (more uniform temperature) and improvements in safety. Conversely, the disadvantages include many interconnections, higher integration and assembly cost, lower weight and volume efficiency and lower reliability. In addition, a large quantity of cell protection and monitoring circuit boards are needed. [43].

On the other hand, using larger cells has several advantages such as lower assembly cost, higher weight and volume efficiency, higher reliability, less complex interconnections and ease of troubleshooting [43]. The disadvantages include higher cell production costs, a tendency to thermal aging (high gradient of temperature across the cell), lower quality and increased difficulties in thermal management. The system will also be prone to safety issues and also needs a complicated and expensive battery protection circuit (high ampere current sensor and used of MOSFET instead of relays) [43].

In this section, integration issues of two different sizes of cylindrical cell will also be explored. The benchmarking of the 38,120 and 18,650 cells is based on the converted EV using the Hyundai Trajet. A relative score of "better than" (+) or "worsen than" (−) is used to represent how the subjective criterion is rated in comparing two different sizes of cells. The assembly of 38,120 and 18,650 cell unit is shown in Fig. 13. The comparison of the cell integration issues from various aspects is tabulated in Table 4.

Manufacturing technology for small cells is more mature than the large cell and the price is cheaper for mass purchasing. In addition, the total number of 18,650 cells (5040 cells) is 6 times higher than the total number of 38,120 cells (784 cells) in the designed battery pack. The total weight of 18,650 cells is 201.6 kg, while the total weight of 38,120 cells is 278.32 kg. This is due to the thick metal pieces used for 38,120 cell threaded terminals. The total

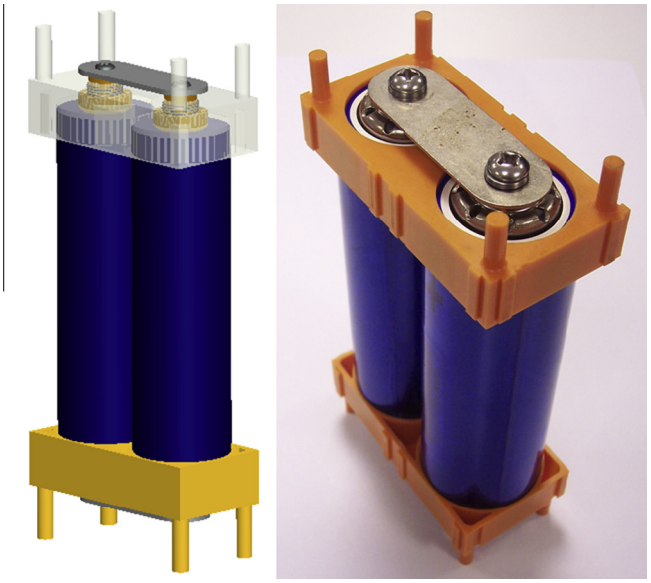

Fig. 13. Assembly of the cells. Left: 18,650 cell. Right: 38,120 cell.

Table 4
Selection and integration issues of 18,650 and 38,120 cell for battery pack.

Criteria	Cell	
	18,650	38,120
Packaging		
Number of cell	5040	784
Weight, kg	201.6	278.32
Volume, m^3 (closed pack)	0.106	0.150
Weight of bus bar, kg	20.26	12.45
Weight of cell holder, kg	~30	~9
Weight of terminal connector, kg	12.13	–
Cell cost, USD	3–5	~20
Assembly of single cell		
α, β orientation of cell [36]	360°, 0°	360°, 0°
Cell handling + insertion time, s [36]	3.5	3.5
α, β orientation of bus bar [36]	180°, 180°	180°, 180°
Bus bar handling + insertion time per cell, s [36]	15.72	15.72
α, β orientation of cell holder [36]	360°, 360°	360°, 360°
Cell holder handling + insertion time, s [36]	7.4	7.4
α, β orientation of terminal connector [36]	360°, 0°	–
Terminal connectors handling + insertion time, s [36]	6.6	–
Bus bar assembly time (two terminal), s [36]	46.36	46.36
Assembly cost, USD (assumed 5 USD per hour)	0.111	0.101
Electrical and control		
Terminal contact resistance, mΩ	10	0.6
Complexity of wiring	1	7/45
Cell monitoring	–	+
Reliability	+	–
Thermal management		
Gradient of internal temperature, °C (Based on US06 cycle)	4	6
Heat generated from contact resistance, kJ/cycle (based on US06 cycle)	208.674	74.08
Heat generated from the battery pack, kJ/cycle (based on US06 cycle)	870.485	780.543
Power consumption for cooling fan	1	0.77
Complexity of cooling system design, cell/m^2	3086	693
Maintenance and troubleshooting		
Time required to identify the faulty cell in the parallel bank	1	7/45
Ease of cell replacement and services	1	7/45

weight of 18,650 cell battery pack increased to 264 kg when bus bar, terminal connectors and plastic cell holder are installed, while features such as the battery pack support structure, thermal management system, battery protection circuit board and wiring are excluded. The total weight of the 38,120 cell battery pack is about 300 kg and it is much heavier than 18,650 cell battery pack. Furthermore, smaller cells have better packing density and power density as compared to larger cells. Therefore, from the packaging point of view, smaller cell is better for battery pack integration. The weight of large cell could be improved by using different material for battery casing and cell terminals.

Most of the products are manually assembled and Boothroyd Dewhurst DFA method for manual assembly is widely used to assess the assembly efficiency. More than 50% of the total manufacturing cost and nearly 60% of the total production time are spent on the assembly process [45–47]. For manual assembly study, the analysis is split into two distinct analyses, which are known as manual handling and insertion analysis respectively. In this study, orientation, part size, ease of handling, types of cell fastener, bus bar and terminal connector are examined to determine the handling and insertion time. α rotation refers to the alignment of the axis of the part corresponded to the axis of insertion, while the rotation of the part about its axis of rotation is called β rotation. In the analysis, the assembly of a single cell is taken into consideration. The labor cost of the assembly is assumed as USD 5 per hour. The total assembly cost of the battery pack excluding battery management system can be calculated by multiplying the number of cell, battery holder and bus bar used. The analysis results are tabulated into the assembly section of Table 4. The total assembly cost of a single 18,650 cell required USD 0.111 while the assembly of a single 38,120 cell required USD 0.101. For the 18,650 cell battery pack that consists of 5040 cells, about USD 559 and 112 h of workmanship are needed for cell assembly and this excludes the assembly of thermal management system, battery protection circuit board and wiring. On the other hand, a 38,120 cell battery pack only required USD 79 and 15.84 h of workmanship. Despite the differences in assembly time, the 18,650 and 38,120 cells actually share the similar characteristic of assembly in term of α and β rotation.

Another difference in the mechanical aspect is the use of terminal connectors. Threaded terminals are provided for 38,120 cells and no terminal connectors are required to assemble 38,120 cells. On the other hand, the 18,650 cells require spring- loaded terminal connectors to bridge the cell terminal to the bus bar. Hence, an additional component and assembly process are involved for the 18,650 cells. This will incur extra manufacturing and assembly cost. As such, in the assembly point of view, the large cell has better assembly efficiency than the smaller cell and the total production time can be shortened effectively to produce a more economical battery pack.

From the electrical aspect, an increasing number of cells also mean that the number of terminal connectors, bus bars and the interconnections are proportionally increased. Furthermore, this will increase the complexity in wiring, copper loss, causing difficulty in cell monitoring and protection circuit design. In the consideration of design for assembly and disassembly, spring-loaded terminal connectors are chosen over spot welding on nickel strip for 18,650 cells assembly. Nevertheless, it will produce a higher value of contact resistance and more energy is wasted in copper loss, which means that the total usable energy of the battery pack is reduced. Moreover, a large number of cells also indicate a large quantity of cell protection and monitoring circuit board is needed. Although a large cell requires less cell protection and monitoring of the circuit board, the circuit design is more complicated and involves high current electronic devices such as the high ampere current sensor and thick interconnections. Moreover, cell balancing (active and passive) is more difficult for a large cell. From the electrical point of view, wiring for a large cell is less complex and copper loss can be reduced to a minimum. Furthermore, the large number of interconnections will increase the chances of failure and make it more difficult for troubleshooting. Hence, from the control point of view, fewer cell protections and monitoring board are needed for large cells and this makes the control task easier. On the other hand, having more cells connected in parallel is expected to increase the reliability of the battery pack and the effect of bad cell could be minimized [48,49]. Cells with the same chemistry have the same mean time between failures. For example, either size of the cells has about 1% likelihood of sudden lose of capacity due to internal failure or external wiring problem over a month. The studied showed that after 10 months, the battery pack with more cells connected in parallel is less influenced by capacity fading [48,49].

US06 driving cycle is used as a reference to assess the thermal performance of 38,120 and 18,650 cell battery packs. The heat generated from 18,650 and 38,120 cells is 870.485 kJ/cycle and 780.543 kJ/cycle respectively. In the 18,650 cell battery pack, the heat is shared equally in 5040 cells. On the other hand, in the 38,120 cell battery pack, the heat is only shared with 784 cells and the thermal problem is more serious for large cell. Due to the small number of interconnections in the 38,120 battery pack, the heat generated from the contact resistance is also small which

is about 74.08 kJ/cycle and 2.8 times less than the heat generated from the contact resistance of the 18,650 cell battery pack. Power consumption for cooling fan is calculated using Eq. (10) [17] and an 18,650 cell battery pack is used as a reference for comparison.

$$h_{forced} = 30\left(\frac{\dot{m}/\rho_{air}A}{5}\right)^{0.8} \quad (10)$$

Axial cooling architecture is used to benchmark the power consumption for the cooling fan. 18,650 cells are stacked in two layers to achieve the similar length with the 38,120 cells. Due to poor packing density of the 38,120 cell battery pack as discussed in Section 3.5, for a given mass flow rate of cooling air, heat transfer coefficient is only 0.77 times less than the 18,650 cell battery pack. Conversely, using a large number of small cells rapidly increases the complexity and the cost of the battery thermal management system design and the assembly of the cells [43]. For the axial cooling architecture, there will be 3086 pieces of 18,650 cell and 693 pieces of 38,120 cells in one square meter. The manifold of the 18,650 cell battery pack needs to take care about 4.5 times more cells than the manifold of the 38,120 cell battery pack. Hence, the design of the 18,650 cell battery pack manifold and ducting is more complex and challenging to ensure the uniformity of temperature distribution. The only concern is that the thermal management for a large cell is the thermal resistance in the cell. Heat is trapped in the cell and this leads to the development of a large temperature gradient. This produces an uncontrollable cell internal temperature, which will give rise to safety and thermal aging issues. Hence, from the thermal perspective, a cell with a large surface area to volume of active material is desired, such as thick and short cylindrical cell or thin and long cylindrical cell as it could help to dissipate the heat more effectively. On the other hand, long electron current path of the thin cylindrical cell, may lead to performance degradation and shorten the cycle life of the cell [43]. The placement of the current tab in thick and short cylindrical cells is a critical issue and needs to be optimized to result in an even current distribution in the active material. Besides, making the cell thinner, such as by changing to the pouch cell design, is more favorable for thermal management.

In addition, a large number of cells make the troubleshooting and maintenance jobs of the battery pack tedious. This type of battery pack is more suitable for use as in "use and throw" products. It does not encourage recycling or repair, and is not environment friendly. On the other hand, the replacement of faulty cells for the battery pack using large cells and the servicing of faulty cell is also easier. For example, in the 18,650 cell battery pack, there will be 180 cells connected in parallel to form a module. On the other hand, there will be only 28 cells connected in parallel for the 38,120 cell battery pack. The time required to detect the faulty cell for the 18,650 cell module is 6 times more than 38,120 cell module. Hence, a large cell is more favorable for maintenance point of view.

By reviewing the integration issues of 18,650 and 38,120 cells, it is apparent that the large cell has extra advantages over the smaller cell. It should also be noted that the large cells tend to develop, a large gradient of temperature, which is associated with thermal aging issues. This problem, however, could be easily alleviated using an internal cooling approach.

4. Conclusions

A detailed battery model is developed to investigate the performance and thermal response of two different sizes of the cylindrical cell. The model is based on the modified Shepherd model by extracting the data obtained from 0.2 I_t-rate of constant current discharge curve is able to predict dynamic behavior of the cell with good accuracy. Detailed information about the battery operating parameters such as SOC, I–V characteristics, skin temperature and internal temperature of the cell can be obtained. The simulation results showed a good agreement with experimental data under various operating conditions. Heat generated in the cell is positively correlated with the I_t-rates and diameter of the cell. Heat exchange surface area per unit volume of the cell is a critical factor that determined the heat dissipation rate from the cell to the external environment.

As the ratio of surface area to volume is reduced, the heat transfer decreases and the internal temperature rises. The maximum temperature region inside the cell is located in the circular region of active material near the hollow core. Due to the large thermal resistance and insulation effect of the separator, the temperature difference of the cell in the radial direction is significant and it increases with the diameter of the cell. This contributes to the slow rise of large cell skin temperature. Smaller sizes have better temperature distribution in the cell. Therefore, measuring skin temperature of the cell is not sufficient as a safety reference for cell operation.

Strong forced convection cooling should be avoided as it will increase the cell internal temperature gradient and accelerate the rate of thermal aging. Other than cost, the electrical, thermal, mechanical, cell assembly and maintenance aspects are the issues that need to be addressed in the cells integration. These issues will further determine the performance, cost and life cycle of the battery pack. Smaller cells allow easier thermal management, but result in a high number of interconnections and an increase in the chance of failure. Large cells perform better in term of assembly efficiency, cell monitoring and maintenance, but perform poorly in thermal management. Due to the growing in Li-ion cell industry and manufacturing technology, cell cost is no longer an issue. An improvement of the cell internal structure, however, is still a need to allow the heat to be dissipated quickly so that a large size and capacity cell can be built.

References

[1] Pesaran AA. Battery thermal management in EVs and HEVs: issues and solutions. In: Proc advanced automotive battery conference. Las Vegas, Nevada; 2001.
[2] Pesaran AA, Smith K, Markel T. Impact of the 3Cs of batteries on PHEV value proposition. In: 9th proc. advanced automotive battery and EC capacitor conference. Long Beach, California; 2009.
[3] Saw LH, Ye Y, Tay AAO. Electrochemical-thermal analysis of 18,650 Lithium Iron Phosphate cell. J Energy Convers Manage 2013;75:162–74.
[4] Heckenberger T. Li-ion battery cooling more than just another cooling task. Stuttgart, Germany: Behr; 2009.
[5] Awarke A, Jaeger M, Pischinger S. Comparison of model predictions with temperature data sensed on board from the Li-ion polymer cells of an electric vehicle. SAE. Int. 2012. http://dx.doi.org/10.4271/2011-01-2443.
[6] Gu WB, Wang CY, Liaw BY. The use of computer simulation in the evaluation of electric vehicle batteries. J Power Sources 1998;75:151–61.
[7] Smith KA, Rahn CD, Wang CY. Control oriented 1D electrochemical model of lithium ion battery. J Energy Convers Manage 2007;48:2565–78.
[8] Smith K, Wang CY. Power and thermal characterization of a lithium-ion battery pack for hybrid electric vehicles. J Power Sources 2006;160:662–73.
[9] Kim GH, Pesaran AA, Spotnitz R. A three-dimensional thermal abuse model for lithium-ion cells. J Power Sources 2007;170:476–89.
[10] Doyle M, Newman J. Comparison of modeling predictions with experimental data from plastic lithium ion cells. J Electrochem Soc 1996;143:1890–903.
[11] Menard L, Fontes G, Astier S. Dynamic energy model of a lithium-ion battery. Math Comput Simul 2010;81:327–39.
[12] Jeon DH, Baek SM. Thermal modeling of cylindrical lithium ion battery during discharge cycle. J Energy Convers Manage 2011;52:2973–81.
[13] Srinivasan V, Wang CY. Analysis of electrochemical and thermal behavior of Li-ion cells. J Electrochem Soc 2003;150:A98–A106.
[14] Gerver RE, Meyers JP. Three-dimensional modeling of electrochemical performance and heat generation of lithium-ion batteries in tabbed planar configurations. J Electrochem Soc 2011;158:A835–43.
[15] Awarke A, Pischinger S, Ogrzewalla J. Pseudo 3D modeling and analysis of the SEI growth distribution in large format Li-ion polymer pouch cells. J Electrochem Soc 2013;160:A172–81.

[16] Moura SJ, Stein JL, Fathy HK. Battery health conscious power management in plug-in hybrid electric vehicles via electrochemical modeling and stochastic control. IEEE Trans Control Syst Technol 2012;21:679–94.
[17] Pesaran AA. Battery thermal models for hybrid vehicle simulations. J Power Sources 2002;110:377–82.
[18] Hu X, Li S, Peng H. A comparative study of equivalent circuit models for Li-ion batteries. J Power Sources 2012;198:359–67.
[19] Moss PL, Au G, Plichta EJ, Zheng JP. An electrical circuit model for dynamic performance of Li-ion polymer batteries. J Electrochem Soc 2008;155:A986–94.
[20] Gonzalez-Longatt FM. Circuit based battery models: a review. In: 2nd CIBELEC 2006. Puerto La Cruz, Venezuela; 2006.
[21] He H, Xiong R, Guo H. Online estimation of model parameters and state-of-charge of $LiFePO_4$ batteries in electric vehicles. J Appl Energy 2012;89:413–20.
[22] Sun F, Xiong R, He H, Li W, Aussems JEE. Model-based dynamic multi-parameter method for peak power estimation of lithium-ion batteries. J Appl Energy 2012;96:378–86.
[23] Tong SJ, Same A, Kootstra MA, Park JW. Off-grid photovoltaic vehicle charge using second life lithium batteries: an experimental and numerical investigation. J. Appl Energy 2013;104:740–50.
[24] Xiong R, Sun F, Gong X, Gao C. A data-driven based adaptive state of charge estimator of lithium-ion polymer battery used in electric vehicles. J Appl Energy 2014;113:1421–33.
[25] Xiong R, Sun F, Chen Z, He H. A data driven multi-scale extended Kalman filtering based parameter and state estimation approach of lithium-ion polymer battery in electric vehicles. J Appl Energy 2014;113:463–76.
[26] Xing Y, He W, Pecht M, Tsui KL. State of charge estimation of lithium-ion batteries using the open-circuit voltage at various ambient temperatures. J Appl Energy 2014;113:106–15.
[27] Waag W, Sauer DU. Adaptive estimation of the electromotive force of the lithium-ion battery after current interruption for an accurate state-of-charge and capacity determination. J Appl Energy 2013;111:416–27.
[28] Saw LH, Somasundaram K, Ye Y, Tay AAO. Electro-thermal analysis of Lithium Iron Phosphate battery for electric vehicles. J Power Sources 2014;249:231–8.
[29] Kroeze RC, Krein PT. Electrical battery model for use in dynamic electrical vehicle simulations. In: Proc. power electronics specialists conference; 2008. p. 1336–42.
[30] Chen Y, Evans JW. Three-dimensional thermal modeling of lithium-polymer batteries under galvanostatic discharge and dynamic power profile. J Electrochem Soc 1994;141:2947–55.
[31] Hu X, Sun F, Zou Y. Estimation of state of charge of Lithium-ion battery pack for electric vehicles using an adaptive Luenberger Observer. Energies 2010;3:1586–603.
[32] Kim Y, Ho T, Thelliez M, Tan E. 3D thermal analysis of Li-ion battery cells with various geometries and cooling conditions using Abaqus. In: Proc. simulia community conference. Providence RI, USA; 2012.
[33] Shi J, Wu F, Chen S, Zhang C. Thermal analysis of rapid charging nickel/metal hydride batteries. J Power Sources 2006;157:592–9.
[34] Shepherd CM. Design of primary and secondary cells: II. An equation describing battery discharge. J Electrochem Soc 1965;112:657–64.
[35] Tremblay O, Dessaint L. Experimental validation of a battery dynamic model for EV applications. J WEVA 2009;3.
[36] Tremblay O. A generic battery model for the dynamic simulation of hybrid electric vehicles. In: VPPC 2007, Proc. vehicle power and propulsion conference. Arlington, TX, USA; 2007.
[37] Bernardi D, Pawlikowski E, Newman J. A general energy balance for battery systems. J Electrochem Soc 1985;132:5–12.
[38] Forgez C, Do DV, Friedrich G, Morcrette M, Delacourt C. Thermal modeling of a cylindrical $LiFePO_4$/graphite lithium-ion battery. J Power Sources 2010;195:2961–8.
[39] Chen SC, Wang YY, Wan CC. Thermal analysis of spirally wound lithium batteries. J Electrochem Soc 2006;153:A637–48.
[40] Wang J, Liu P, Hicks-Garner J, Sherman E, Soukiazian S, Verbrugge M, et al. Cycle-life model for graphite-$LiFePO_4$ cells. J Power Sources 2011;196:3942–8.
[41] Han S, Han S, Aki H. A practical battery wear model for electric vehicle charging applications. J Appl Energy 2014;113:1100–8.
[42] Omar N, Monem MA, Firouz Y, Salminen J, Smekens J, Hegazy O, et al. Lithium iron phosphate based battery-assessment of the aging parameters and development of cycle life model. J Appl Energy 2014;113:1575–85.
[43] Pesaran AA, Kim GH, Keyser M. Integration issues of cells into battery packs for plug-in and hybrid electric vehicles. In: Proc. EVS24. Stavanger, Norway; 2009.
[44] Xue N, Du W, Greszler TA, Shyy W, Martins JRRA. Design of a lithium-ion battery pack for PHEV using a hybrid optimization method. J Appl Energy 2014;115:591–602.
[45] Boothroyd G, Dewhurst P, Knight WA. Product design for manufacture and assembly. 3rd ed. New York: CRC Press; 2011.
[46] Edward KL. Towards more strategic product design for manufacture and assembly: priorities for concurrent engineering. Mater Des 2002;23:651–6.
[47] Kim GJ, Bekey GA, Goldberg KY. A shape metric for design-for-assembly. Proc. IEEE Int Conf Rob Autom 1992;2:968–73.
[48] Andrea D. Battery management systems for large lithium-ion battery pack. Massachusetts: Artech House; 2010.
[49] Andrea D. Lots of small cells are better than one big one. Elithion; 2008. Retrieved January 2014. <http://liionbms.com/php/wp_lots_small_cells.php>.